

UC San Diego

UC San Diego Electronic Theses and Dissertations

Title

CDKL5 iPSC-derived Neural Cells Exhibit Deficiencies in Growth and Increased Apoptosis

Permalink

<https://escholarship.org/uc/item/52p0r31r>

Author

Kwok, Ellius

Publication Date

2018

Peer reviewed|Thesis/dissertation

UNIVERSITY OF CALIFORNIA SAN DIEGO

CDKL5 iPSC-derived Neural Cells Exhibit Deficiencies in Growth and Increased
Apoptosis

A thesis submitted in partial satisfaction of the requirements for the degree

Master of Science

in

Biology

by

Ellius Kwok

Committee in Charge:

Alysson Muotri, Chair
Deborah Yelon, Co-Chair
Christopher Armour

2018

The Thesis of Ellius Kwok is approved, and it is acceptable in quality and form for publication on microfilm and electronically:

Co-Chair

Chair

University of California San Diego

2018

DEDICATION

I dedicate this thesis to my family and loved ones. Thank you for your unwavering support and patience through the years.

TABLE OF CONTENTS

Signature page.....	iii
Dedication.....	iv
Table of Contents.....	v
List of Figures.....	vi
List of Tables.....	vii
Acknowledgements.....	viii
Abstract of the Thesis.....	ix
Introduction.....	1
Materials and Methods.....	10
Results.....	19
Discussion.....	25
Figures.....	31
Tables.....	39
References.....	41

LIST OF FIGURES

Figure 1.	Characterization of CDKL5 disorder patient-derived iPSCs and their potential for differentiation.....	32
Figure 2.	NPCs derived from CDKL5 disorder patient iPSCs display decreased levels of proliferation.....	34
Figure 3.	CDKL5 Disorder leads to increased levels of apoptosis in NPCs.....	35
Figure 4.	CDKL disorder iPSC-derived neurons appear to grow more slowly than controls during early development.....	36
Figure 5.	CDKL5 disorder iPSC-derived neurons display a greater density of spines with increased motility.....	37

LIST OF TABLES

Table 1.	CDKL5 Patient Cohort and Controls.....	40
----------	--	----

ACKNOWLEDGEMENTS

Firstly, I would like to acknowledge and thank Dr Alysson R. Muotri for the opportunity to be a part of the work he does in his lab. I have learned so much over the past three years as a member of the Muotri lab and it would not have been possible without his guidance, as well as the guidance of the post-doctoral scholars, graduate students, and other lab personnel.

Secondly, I would like to thank Dr Deborah Yelon and Dr Christopher Armour for their time and effort to be a part of my thesis committee. All the lessons and guidance they have given to me both in and out of the classroom are greatly appreciated.

Last but not least, I would like to thank Dr Priscilla Negraes and Dr Cleber Trujillo. Without their encouragement and mentorship, I would never have even come close to completing this thesis, and I will be forever grateful for their unending patience.

ABSTRACT OF THE THESIS

CDKL5 iPSC-derived Neural Cells Exhibit Deficiencies in Growth and Increased Apoptosis

by

Ellius Kwok

Master of Science in Biology

University of California San Diego, 2018

Professor Alysson R. Muotri, Chair

Professor Deborah Yelon, Co-Chair

Cyclin-dependent kinase-like 5 (CDKL5) syndrome is a neurodevelopmental disorder that results in early-onset intractable seizures, mental retardation, and a host of autistic phenotypes. Although the role of CDKL5 is not well understood, previous studies have implicated it plays a crucial role within the AKT/mTOR pathways, which regulate cellular proliferation, apoptosis, and synaptogenesis. This study focused on generating neural progenitor cells (NPCs) and subsequently differentiating them into neurons, for the

purpose of modeling the effects of CDKL5 mutations on the phenotypes listed above. hiPSC-derived CDKL5 NPCs exhibited decreased cell proliferation and increased apoptosis as compared to controls, which is congruent with the findings of previous studies with regards to inactivation of the AKT/mTOR pathways. Furthermore, hiPSC-derived CDKL5 neurons displayed no change in total dendritic length but appeared to grow more slowly during early neurodevelopment as compared to controls. These neurons also had a greater density of dendritic spines, with increased motility, as compared to controls. These findings conflict with the results from previous CDKL5 studies based on mouse knockout models, which suggests that CDKL5 function may not be preserved across species. This hypothesis is further supported by the fact that the murine models do not recapitulate the defining feature of CDKL5: early-onset intractable seizures.

INTRODUCTION

Disease Modeling

A disease model is an organism that displays the pathology of disease, allowing for further study of its mechanisms and effects, as well as exploration of possible therapies. A variety of different organisms have been employed to model disease, ranging from the unicellular level, such as bacteria and yeast, to high organisms, such as rats and chimpanzees. These models enable researchers to examine the roles of specific genes and how associated disease affects the typical function of cellular pathways (Kobayashi, 2004). One of the largest benefits of non-human disease modeling is that it enables the study of virulent diseases, such as Ebola, without compromising the health of an actual human being (Bente 2009). Mice are a commonly used to model human diseases due to their accessibility and relative ease of care (Bolker, 2012). However, there are some differences in the physiology of mice that limit the translation of findings from mouse studies to humans. Due to these differences, clinical applications of results from these studies have proved modest considering the wide usage of murine models (Herrath, 2005). Physiological differences between mice and humans prove especially significant in the study of neurodevelopment, since the cortices of mice are lissencephalic compared to the sulci and gyri of the human brain (Watase, 2003). Furthermore, the modeling of diseases with a monogenic cause is based on the premise that the gene functions identically in both the model organism as well as humans. However, gene function is not always conserved between species, limiting the accuracy of animal models to recapitulate human diseases (Alessio, 2017). As a result, caution must be employed when extrapolating the significance of results from animal-based disease models on human neurodevelopmental diseases.

One method of bypassing the limitations of animal models for human neurological diseases is to study post-mortem brain tissue. However, post-mortem tissue provides only information about the state of cells at a single point in time and does not allow for the exploration of mechanisms or potential rescue treatments. Also, brain tissue is scarce and is highly dependent on how it is handled during collection; improper harvesting or storage can greatly affect the preservation of DNA, RNA, proteins, and lipids (Ferrer, 2008).

Due to the weaknesses of utilizing nonhuman organisms and post-mortem tissue to model diseases, an alternative method must be identified to mimic the pathophysiology of human diseases. Being able to faithfully model human neurological diseases would validate the findings of nonhuman models and enable further insight to the mechanisms of human neurological diseases.

Stem Cells and Disease Modeling

Human embryonic stem cells (hESCs) have been derived from blastocysts and been shown to have the capacity to differentiate into the three germ layers (Thomson, 1998). These cells provide a platform to study human developmental biology *in vitro* and *in vivo*. However, in order to model human genetic diseases, it is necessary to generate cell lines with dysfunctional genomes. Utilizing genome editing tools can be a viable technique to generate these diseased cell lines, but the ethical concerns surrounding the harvesting of hESCs and the possibility of off-target effects during genome editing lends this method diminished viability. In 2007, Takahashi and colleagues were able to

reprogram human somatic cells into an ESC-like state, known as induced pluripotent stem cells (iPSCs), via overexpression of four transcription factors: Oct4, Sox2, Klf4, and cMyc (Takahashi, 2007). iPSCs are functionally similar to ESCs, being able to proliferate and differentiate into cells types stemming from all three germ layers following exposure to specific growth factors and culture conditions (Ebert, 2012). As such, iPSCs present a viable method of obtaining patient-derived stem cells relatively noninvasively and culturing live cells normally extremely difficult to obtain, such as human cortical neurons. Since the cells are patient-derived, they retain the genomic features and mutations from their source, allowing for accurate modeling of genetic diseases as well as testing of potential therapeutics.

Using iPSC-Derived Neurons to Study Neurodevelopmental Disorders

In order to employ iPSCs as a valid system to model neurodevelopmental disorders, it must be proven that they accurately represent patient brain cells *in vivo*. Researchers studying iPSCs that were differentiated towards the neural lineage specifically examined their regional identity, as well as developmental maturity (Stein, 2014). Through gene expression analysis, they found that the hiPSC-derived neurons displayed an enrichment of cortical cell markers, revealing the strong cortical identity of *in vivo* cultures (Stein, 2014). With regards to developmental maturity, it was found that the hiPSC-derived neurons cultured *in vitro* only matured to approximately the level of *in vivo* mid-fetal neurons (Stein, 2014). However, it was also found that the differentiation and development of hiPSC-derived neurons closely represented that of human neurons *in vivo*, especially with regards to neurodevelopmental processes such as corticogenesis

(Stein, 2014). As such, the limited neuronal maturation and biased cellular identity with this differentiation protocol may render hiPSCs insufficient for modeling late onset neurodegenerative issues or genetic diseases that affect non-cortical areas of the brain. However, for modeling early-onset neurodegenerative diseases, hiPSC-derived neurons remain an avenue of great potential.

In fact, researchers have begun using hiPSCs to study disease phenotypes, neurodevelopmental processes, and potential therapies. One of the earliest examples of these models was when Marchetto and colleagues cultured hiPSC-derived neurons from patients affected with Rett syndrome (RTT) (Marchetto, 2010). Rett syndrome is a debilitating disease that primarily affects young girls, presenting as mental retardation and a lack of development of early skills such as communication, early language, and fine motor control (Bengt, 2002). This disease typically arises due to a mutation in the methyl-CpG-binding protein 2 (MECP2) gene, which is located on the X-chromosome, and results in microcephaly (Amir, 1999), leading to the clinical phenotypes listed above. Marchetto and colleagues reprogrammed fibroblasts donated from RTT patients and differentiated the resulting hiPSCs into neurons. Their neuronal model corroborated findings from previous studies using murine and post-mortem tissue models; RTT affected neurons have smaller somas, less dendritic complexity, and fewer excitatory synaptic connections. The authors took the study a step further and screened for potential therapies, including insulin-like growth factor 1 (IGF-1), which had previously been shown to partially rescue symptoms in MECP2 mutant mice (Tropea, 2009). Their treatment resulted in a rescue of hiPSC-derived RTT neurons; excitatory synapses were able to be restored to levels mirroring that of controls (Marchetto, 2010). This early

model system displays the capability of hiPSC-derived neurons to reproduce neurological and cellular deficits seen in murine and post-mortem brain tissue models, thus validating the use of these cells to model neurodevelopmental disorders.

CDKL 5 Disorder

Mutations in the cyclin dependent kinase-like 5 (CDKL5) gene, located on the X chromosome, leads to the development of CDKL5 syndrome in humans. CDKL5 syndrome is an independent disease that was initially thought to be a subset of Rett syndrome, as patients of both syndromes present many of the same clinical phenotypes (Chen, 2010). This overlap may be due to the fact that the CDKL5 gene is a target of MECP2 (Carouge, 2010). However, beyond the symptoms typical of Rett, CDKL5 syndrome patients present with early onset intractable seizures, a unique and defining trait that led to the standalone classification of this syndrome (Fehr, 2012). The occurrence of early onset seizures results in devastating retardation of the early developmental process, with a severity exceeding that of typical Rett syndrome (Bahi-Buisson, 2008). Due to its location on the X chromosome, mutations of the CDKL5 gene predominantly affects females, with only 10% of the approximately 600 cases reported worldwide corresponding to males. Hemizygous males with a nonfunctional copy of CDKL5 likely display a more severe phenotype than females, who tend to present with a spectrum of phenotypes based on the mosaicism of mutant CDKL5 X-inactivation. Thus far, both male and female CDKL5 patients have displayed a variety of mutations, such as nonsense, missense, frameshift, and splice variants-, all of which generally result in a loss of function of the protein coded by this gene (Bahi-Buisson, 2012).

The CDKL5 gene is located at the Xp22.13 locus, which when translated produces a kinase of unknown function, although studies have indicated that it interacts with the N-terminal domain of DNA methyltransferase 1 in mouse brains (Kameshita, 2008). DNA methyltransferase 1 is primarily responsible for histone methylation in the mammalian genome, allowing for such events as gene silencing and X-chromosome inactivation (Bestor, 2009). This important role in gene regulation gives a possible explanation to the wide range of adverse clinical features that arise from the loss of proper function a protein that underpins such critical functions of cellular development. Another interaction that researchers have elucidated is the possible role of the CDKL5 protein in the mechanistic target of rapamycin (mTOR) pathway. A study done using a mouse knockout model was able to replicate the autistic behavioral phenotypes of CDKL5 syndrome, as well as measured brain responses (Wang, 2012). However, in this study researchers were unable to reproduce the critical clinical feature of CDKL5 in humans, early onset seizures, suggesting that this disease may not function within mice as it does in humans. Experiments performed using this model found a disruption of multiple cellular signaling pathways, most notably the phosphorylation of several upstream elements of mTOR; mutations in CDKL5 were shown to cause decreased phosphorylation of adenosine monophosphate-activated protein kinase (AMPK) and protein kinase B (AKT). The mTOR pathway has been implicated in mammals as critical for cellular growth and development of cells, controlling many essential functions such as synthesis of proteins and lipids, as well as cellular metabolism (Laplante & Sabatini, 2012). Using rodent models, mTOR was shown to also be involved in the regulation of the maturation and arborization of neurons (Cammelleri, 2003; Grider, 2009), suggesting

a causal link between CDKL5 misregulation, mTOR dysfunction, and abnormal brain development.

Several studies have attempted to explore links between CDKL5 protein function and other pathways that underpin cell development. Thus far, studies have been focused on using mouse knockout models to examine the role of CDKL5 in brain development. Fuchs et al. found that dendritic development and growth was impaired in CDKL5 knockout mice and suggested connections to the AKT pathway, an upstream signaling pathway for mTOR as discussed previously (Fuchs, 2014). Amendola et al. found that CDKL5 knockout produced mice with reduced dendritic length and cortical thickness (Amendola, 2014). These researchers also implicate the AKT pathway as a possible cause of these deficiencies and show links between CDKL5 syndrome and abnormal brain development. Furthermore, La Montanara et al. examined the phosphorylation levels of proteins along the mTOR pathway using the mouse CDKL5 knockout model and found hypo-phosphorylation of mTOR substrates (La Montanara, 2015).

Modeling CDKL5 Using hiPSCs

Human induced pluripotent stem cells (hiPSCs) represent another avenue to study the effects of CDKL5 syndrome on neuronal development. As stated previously, the generation of stem cell lines derived from patient fibroblasts is a relatively non-invasive method of obtaining living CDKL5 neurons *in vitro*. Furthermore, due to the X-linked nature of CDKL5 syndrome, isogenic cell lines can be derived from female patients, offering the ability to compare cells that are genetically identical except for the mutation

of the CDKL5 gene. Only one study has previously utilized human derived cells to determine the effects of CDKL5 on human neuronal development. Although most of their experiments were conducted using a mouse knockout model, Ricciardi et al. also uses hiPSCs to study the effects of CDKL5 on human cells *in vitro* and found that mutations in the CDKL5 gene led to decreased spine density and synapse formation (Ricciardi 2012).

Beyond the study by Ricciardi however, no other studies have explored the effects of CDKL5 mutations on the development and morphology of human neurons, especially using patient derived cells. The predominance of mouse models that do not fully recapitulate the clinical phenotypes of human CDKL5 syndrome patients, especially the defining feature of early onset seizures, entails further testing utilizing models with a human origin. Thus, using patient derived hiPSCs as a model, this study aims to explore how CDKL5 syndrome affects the AKT and mTOR pathways through examining their effects downstream on neuronal cell outgrowth, proliferation, and apoptotic rate.

MATERIALS AND METHODS

Patient Consent

Upon obtaining informed consent from CDKL5-mutant patients and associated control subjects, fibroblasts were obtained via dermal biopsies under protocols approved by the University of California San Diego Institutional Review Board (#141223).

Cell Culture and Neuronal Differentiation

hiPSCs were cultured on polystyrene dishes (Corning, 430166) coated with Matrigel and mTeSR1 media (Stem Cell Technologies, 5850) was added daily. In order to induce development into the neural lineage, mTeSR media was replaced with N2 media (DMEM/F12 50/50 (Corning Cellgro, 15-090-CV) with 1% HEPES (VWR International, 45000-694), 1% Penicillin Streptomycin (Life Technologies, 15140163), 1% GlutaMAX (Life Technologies, 35050061), and 0.5% N2 Neuroplex (Gemini Bio-products, 400163)), supplemented with 1 μ M dorsomorphin (Tocris 3093) and 10 μ M SB431542 (Stemgent 040010), for 1-2 days. iPSC colonies were then lifted off the plate and cultured in suspension on a cell shaker (95 r.p.m. at 37°C) for eight days to form embryoid bodies (EBs). EBs are then plated on matrigel-coated dishes in NG media (DMEM/F12 50/50 (Corning Cellgro, 15-090-CV) with 1% HEPES (VWR International, 45000-694), 1% Penicillin Streptomycin (Life Technologies, 15140163), 1% GlutaMAX (Life Technologies, 35050061), 0.5% N2 Neuroplex (Gemini Bio-products, 400163), and 1% Gem21 Neuroplex (Gemini Bio-products 400160), supplemented with 20ng/mL human fibroblast growth factor (FGF) (R&D Systems, 414-TE). Neural rosettes that emerged were manually lifted from the dish, dissociated completely using StemPro Accutase (Life Technologies, A11105-01), and plated on 10 μ g/mL poly-L-ornithine

(Sigma-Aldrich, P3655) and 2.5µg/mL laminin (Life Technologies, 23017015) coated plates. The resulting NPCs were cultured in NG media supplemented with 20ng/mL FGF, which was replaced every other day. In order to induce differentiation of the NPCs into neurons, FGF was withdrawn from the NG media and 5µM Rock Inhibitor (Fisher Scientific, 125410) was added for 48 hours.

Immunocytochemistry

2D cultured cells were washed with Dulbecco's Phosphate Buffered Saline (DPBS) (Corning, 21-031-CV) and DPBS/4% paraformaldehyde (PFA) (Core Bio, 19943) was added for 15 minutes. Upon removal of the PFA, the cells were washed three times and then permeabilized using DPBS/0.1% Triton X-100 (Promega, H5412) for 20 minutes at room temperature. A blocking solution consisting of DPBS/3% Bovine Serum Albumin (BSA) (Gemini Bioproducts, 700-110) was added for one hour at room temperature. Primary and secondary antibodies were diluted in this blocking solution. Cells were incubated with the primary antibody at 4°C for 18 hours. After incubation with the primary antibody solution, the cells were washed three times with DPBS before the secondary antibody solution was added for 1 hour. The cells were again washed three times before a 1:10,000 DAPI:DPBS solution was added (VWR International, 80051-386) for 7 minutes at room temperature. Following removal of the DAPI solution, the cells were washed three times with DPBS and the slides were mounted using Prolong Gold Antifade Reagent (Life Technologies, P36930) and covered with a glass coverslip (Fisher Scientific, 1255015).

Primary antibodies used for immunocytochemistry are as follows: Anti-Tra-1-60 (abcam, ab16288, 1:250), anti-Oct4 (abcam, ab19857, 1:500), anti-H3K27me3 (abcam, ab6002, 1:1000), anti-Nestin (Millipore, ABD69, 1:250), anti-Sox2 (abcam, ab75485, 1:250), anti-Map2 (abcam, ab5392, 1:1000), and anti-Synapsin (Millipore, AB1543P, 1:500). Secondary antibodies conjugated to Alexa Fluors 488, 555, 647 were used at a dilution of 1:1000 (Life Technologies).

RNA Extraction and RT-PCR (iPSC)

RNA was extracted using the QIAGEN RNeasy Plus Mini Kit (Qiagen, 74134). The extracted RNA was quantified using the Nanodrop (Thermo Fisher).

RNA Extraction and Quantification (NPC)

2D cultured NPCs were washed with DPBS (Corning, 21-031-CV) and chemically dissociated using Stempro Accutase (Life Technologies, A11105-01). 1×10^6 cells were pelleted and 1mL Trizol reagent was added. The samples were incubated at room temperature for 5 minutes, following which 200 μ L of chloroform was added and the solution vortexed. After a 3 minute incubation at room temperature, the samples were centrifuged at 12,000 g for 15 minutes at 4°C. After centrifugation the solution will have separated into three distinct layers, of which the topmost aqueous layer was transferred to a new microtube. 500 μ L of isopropanol was then added to each microtube and incubated at room temperature for 10 minutes. The samples were then centrifuged at 12,000 g for 10 minutes at 4°C. Following centrifugation, supernatant was aspirated and the samples washed with 1mL of 75% EtOH. The samples were then centrifuged at 7,500 g for 5

minutes at 4°C. The 75% EtOH was aspirated and the pellet was resuspended in 20 µL RNase Free H₂O, then quantified using the Nanodrop (Thermo Fisher).

Protein Extraction and Quantification

One tablet of PhosSTOP (Roche, 04906837001) and cOmplete Ultra (Roche, 05892791001) was added to 10mL of RIPA buffer (Thermo Scientific, 89901). 100 µL of the RIPA buffer solution was added to 1×10^6 NPCs in 1.5mL microtubes (Thermo Fisher Scientific, 05-408-129), and vortexed to mix before being left on ice for 15 minutes. Samples were then sonicated for 5 minutes at 4°C. After sonication, samples were centrifuged at 12,000 rcf in a centrifuge that was precooled to 4°C. The resultant supernatant was transferred to a new microtube and quantified using the Pierce BCA Protein Assay Kit (Thermo Fisher Scientific, 23225).

DAPI Staining (DNA Fragmentation and Cell Cycle)

2D cultured NPCs were washed with DPBS (Corning, 21-031-CV) and chemically dissociated using Stempro Accutase (Life Technologies, A11105-01). 1×10^6 - 2×10^6 cells were transferred and resuspended in 0.5 mL of DPBS. 4.5 mL of 70% ethanol was then added on ice and the samples were vortexed and stored for 24 hours. The samples were then vortexed and the ethanol was removed, followed by one wash using 5 mL of DPBS. The cells were then resuspended in 0.5 mL DAPI staining solution (Chemometec, 910-3003). The cell solution was loaded into A8 NC-slides (Chemometec, 942-0003) and analyzed immediately using the NC-3000 Advanced Image Cytometer

(Chemometec, 970-3002). Cells prepared in this manner were used to determine the level of DNA fragmentation as well as cell cycle stages in NPCs.

JC-1 Staining (Mitochondrial Dysfunction)

2D cultured NPCs were washed with DPBS (Corning, 21-031-CV) and chemically dissociated using Stempro Accutase (Life Technologies, A11105-01). Approximately 1×10^6 cells were resuspended in DPBS and 12.5 μL of 200 $\mu\text{L}/\text{mL}$ JC-1 solution (ChemoMetec, 910-3007) was added before incubating at 37°C for 10 minutes. The cells were washed twice with DPBS, then 250 μL of 1 $\mu\text{g}/\text{mL}$ DAPI solution (ChemoMetec, 910-3008) was added. 10 μL of the resulting solution was added to each chamber of a A8 NC-slide (Chemometec, 942-0003). The slides were analyzed using the NC-3000 Advanced Image Cytometer (Chemometec, 970-3002). Cells prepared in this manner were used to determine the level of dysfunctional mitochondria in NPCs.

Caspase Staining (Apoptosis)

2D cultured NPCs were washed with DPBS (Corning, 21-031-CV), chemically dissociated using Stempro Accutase (Life Technologies, A11105-01), and diluted to a concentration of 2×10^6 - 5×10^6 cells/mL using DPBS. 5 μL of FLICA reagent (ImmunoChemistry Technologies, 93) was then added to 93 μL of the cell suspension. 2 μL of 500 $\mu\text{g}/\text{mL}$ Hoechst 33342 (ChemoMetec, 910-3015) was also added, and the resultant solution was incubated at 37°C for one hour. After the incubation, the cells were washed twice with apoptosis wash buffer (ImmunoChemistry Technologies, 93) before being resuspended in 100 μL of the apoptosis wash buffer and 2 μL of 100 $\mu\text{g}/\text{mL}$ of

propidium iodide (ChemoMetec, 910-3016). 30 μ L of solution was then loaded into each chamber of an A2 NC-Slide (Chemometec, 942-0001). The slides were then analyzed using the NC-3000 Advanced Image Cytometer (Chemometec, 970-3002).

Annexin Staining

2D cultured NPCs were washed with DPBS (Corning, 21-031-CV) and chemically dissociated using Stempro Accutase (Life Technologies, A11105-01). 2×10^5 - 4×10^5 cells were transferred and resuspended in 100 μ L of Annexin V Binding Buffer (Biotium, 99902). 2 μ L of Annexin V-CF488A Conjugate (Biotium, 29005) and 2 μ L of 500 μ g/mL Hoechst 33342 (ChemoMetec, 910-3015) was added before incubating at 37°C for 15 minutes. The cells were then washed twice using 300 μ L of Annexin V Binding Buffer before being resuspending in 100 μ L of the binding buffer with 2 μ L of propidium iodide (ChemoMetec, 910-3016). 30 μ L of the resulting solution was loaded into each chamber of an A2 NC-slide and analyzed using the NC-3000 Advanced Image Cytometer (Chemometec, 970-3002).

Imaging Neural Progenitor Cell Proliferation

2D cultured NPCs were washed with DPBS (Corning, 21-031-CV) and chemically dissociated using Stempro Accutase (Life Technologies, A11105-01). 4.5×10^5 cells were resuspended in NGF media, then transferred and plated onto 35mm No. 1.0 Coverslip Glass Bottom Dishes (MatTek, P35G-1.0-14-C) coated with 10 μ g/mL poly-L-ornithine (Sigma-Aldrich, P3655) and 2.5 μ g/mL laminin (Life Technologies, 23017015). The plates were placed in a 37°C incubator for four hours to allow attachment before they

were loaded into Viva View FL Incubator Microscope (Olympus). Images (367 μ m by 327 μ m) were taken at 1 hour intervals for a total of 48 hours. Cells that displayed the typical NPC shape were then counted manually at 12 hour time intervals using the Cell Counter plugin on the Fiji platform (Schindelin, 2012).

Live Imaging of Neurite Outgrowth

14 day neurons were washed with DPBS (Corning, 21-031-CV) and chemically dissociated using a 1:1 mixture of Stempro Accutase (Life Technologies, A11105-01) and Accumax (Innovative Cell Technologies, AM 105) for 20 minutes. The neurons were passed through a cell strainer (Fisher Scientific, 87711) and resuspended in NG media. 2.5×10^4 cells were then transferred and plated onto the center of a 35mm No. 1.0 Coverslip Glass Bottom Dishes (MatTek, P35G-1.0-14-C) coated with 10 μ g/mL poly-L-ornithine (Sigma-Aldrich, P3655) and 2.5 μ g/mL laminin (Life Technologies, 23017015). The plates were placed in a 37 $^{\circ}$ C incubator for four hours to allow attachment before 2.5mL of NG media was added to cover the rest of the dish. The dishes were then loaded into Viva View FL Incubator Microscope (Olympus) for imaging. Images were taken at 1 hour intervals for a total of 48 hours. Neurons that were determined to have neurites longer than the neuronal cell body were tracked and their neurites traced at 12 hour time intervals. The tracing was performed using the NeuronJ plugin (Meijering, 2004) on the Fiji platform (Schindelin, 2012).

Lentiviral Transduction

Neurons were transduced with a Synapsin-1 (Syn) promoter upstream of an EGFP reporter in a lentiviral backbone (Nageshappa 2015). Multiplicity of infection (MOI) for this transduction was approximately 2. They were then cultured for 2 more weeks before imaging using a fluorescence microscope (Zeiss, Z1 Axio Observer Apotome)

Neuronal Spine Analysis

Images from GFP-labeled 8 week neurons (see **Lentiviral Transduction**) were analyzed using the (Meijering, 2004) on the Fiji platform (Schindelin, 2012). Only neurons that displayed at least 2 neurites with visible spines at t=0 were considered for analysis.

Statistical Analysis

Both technical and biological replicates were used to determine standard error, with N displayed in the respective figure captions. Data distribution was assumed to be normal and no statistical methods were used to determine sample sizes. Standard spreadsheet software (Microsoft Excel) was utilized to organize raw data, which was then graphed using Graphpad Prism (Graphpad Software, v5.01). Prism was used to determine the Standard Error of the Mean (S.E.M) as depicted by the error bars on each figure. For *t*-test analysis, two-tailed, unpaired tests were used with $\alpha = 0.05$.

RESULTS

Characterization of CDKL5 disorder patient-derived iPSCs and their potential for differentiation.

For this study, four pairs of cell lines were used, which stem from patients with CDKL5 disorder and either isogenic (female) or family-related controls (**Table 1**). Two of the patient cell lines featured a premature nonsense mutation, resulting in a loss of function and no CDKL5 protein produced, whereas another contained a splicing mutation in Exon 7, resulting in production of abnormal CDKL5 protein (**Fig 1A**). The final cell line pair is an isogenic cell line and its related control, which were generated utilizing the X inactivation of a heterozygous CDKL5 syndrome female patient. To characterize iPSCs and their subsequent cell types from along the neural induction pathway (**Fig 1B**), cells were stained and visualized. iPSCs were tested for pluripotency and histone methylation markers (**Fig 1C-D**), to ensure their potential for differentiation and the legitimacy of the isogenic cell line. To further corroborate the characterization of the iPSCs, a comparison of the relative gene expression of markers from each of the three cell lineages, as well as two pluripotency markers, was performed between iPSCs and EBs (**Fig 1E**). The EBs were found to have a significantly greater level of expression for Alpha-fetoprotein (AFP, endoderm marker), Nestin (NES, ectoderm marker), and Msh Homeobox 1 (MSX1, mesoderm marker), and a much lower level of expression for LIN28 and NANOG (pluripotency markers). The identity of the neural progenitor cells (NPCs) and neurons generated from these iPSCs were also confirmed via their respective cell markers (**Fig 1F-G**), thus concluding that the patient-derived iPSCs were functional and capable of producing NPCs and neurons for study.

NPCs derived from CDKL5 disorder patient iPSCs display decreased levels of proliferation.

Due to the findings of previous studies linking the mTOR pathway with cellular growth (Laplante & Sabatini, 2012), as well as suggesting that CDKL5 may play an important role along this pathway (Wang, 2012), NPCs were examined for aberrations in cellular growth and proliferation. Plated NPCs were live imaged over a 48-hour time course at one hour intervals (**Fig 2A**). When the results were pooled and compared over a 24-hour period, CDKL5 disorder patient-derived NPCs (CDKL5 NPCs) were found to proliferate at a slower rate compared to controls (**Fig 2B**). To investigate further into the potential differences in cell growth, NPCs were stained with DAPI, which intercalate with DNA and can be used to compare relative amounts of DNA within each cell (**Fig 2C**). By comparing the intensity of the DAPI staining and the typical distribution of DNA of cells within various stages of the cell cycle, the percentage of cells within each stage can be determined (**Fig 2C**). CDKL5 NPCs were found to have a lower percentage of cells in the late proliferative G2 phase of the cell cycle, and more cells within the early proliferative G1 phase as compared to controls (**Fig 2D**). These data suggest that CDKL5 mutations may lead to disruptions of cellular growth, even in the early stages of neurodevelopment.

CDKL5 Disorder leads to increased levels of apoptosis in NPCs

To further explore the effects of CDKL5 misregulation on early neurodevelopment, assays were performed to examine the levels of cell death in NPCs. A DAPI staining was again performed to determine the percentage of cells that contained less than a full complement of DNA (**Fig 3A**). NPCs generated from the R59X patient

cells lines, a mutation that results in no functional CDKL5 protein, displayed a significantly higher percentage of cells with fragmented DNA as compared to controls (**Fig 3B**), indicating higher levels of cell death. Interestingly, NPCs generated from the D135_F154del patient cell line showed significantly lower percentages of apoptotic cells compared to controls (**Fig 3C**). NPCs generated from the isogenic R550X cell line displayed the same trend as the R59X cell lines, CDKL5 cells had significantly higher levels of apoptosis compared to controls (**Fig 3D**). This discrepancy may be due to the nature of the respective mutations; R59X and R550X lead to truncated proteins, whereas D135_F154del is a splicing mutation that results in an aberrant protein of unknown functionality. To corroborate these findings, a JC-1 staining was performed to determine mitochondrial membrane potential in NPCs (**Fig 3E**), the loss of which is a precursor for apoptosis. R59X NPCs were found to have significantly greater depolarization of mitochondria, which corresponds to a greater number of apoptotic cells compared to controls (**Fig 3F**). The data was normalized to generate fold change data, correcting for any between-trials differences while performing the assay and enabling valid comparison. Similar to the results from the DNA fragmentation assay (**Fig 3A**), D135_F154del NPCs did not display any significant difference in mitochondrial membrane potential as compared to controls (**Fig 3G**). Lastly, caspase activity was analyzed to determine the relative distribution of cells within each of the stages of apoptosis (**Fig 3H**). Once again the R59X NPCs had significantly less healthy cells, and more apoptotic cells than controls, notably a larger proportion in the early apoptotic stage (**Fig 3I**). The D135_F154del NPCs did not display a significant difference in either levels of healthy or apoptotic cells from controls (**Fig 3J**). The increase in apoptosis of the R59X and R550X

mutant NPCs suggests that a lack of CDKL5 protein may lead to increased cell death. However, the D135_F154del NPCs did not exhibit any increased cell death, suggesting that the abnormal protein may still be functioning in some way to prevent this from occurring.

CDKL disorder iPSC-derived neurons appear to grow more slowly than controls during early development.

Studies using mouse CDKL5 knockouts have previously shown that the mutant neurons exhibit impaired dendritic development and growth. In order to examine the effects of the CDKL5 mutations on neurons, patient iPSC-derived NPCs were differentiated for two weeks using the Muotri lab *in-vitro* differentiation protocol, which primarily produces cortical neurons. These neurons were dissociated and re-plated at a low confluency to observe the growth of individual neurites over a 48-hour period (**Fig 4A**). The total length of all neurites from each neuron was measured at various time points, and no significant difference was found between CDKL5 mutant neurons and related controls (**Fig 4B**). However, upon analysis of the growth rates of the neurites, CDKL5 neurons appeared to grow slightly more slowly than controls, as shown by a significant difference between the relative lengths at 12 hours (**Fig 4C-D**). This difference in the fold change of the total neurite length was not replicated at later time points, when the growth rate of control neurites appears to plateau while the growth rate of the CDKL5 neurites appears to stay approximately constant.

CDKL5 neurons display a greater density of spines with increased motility

Mouse studies have also shown that beyond the deficiencies in dendritic growth, CDKL5 neurons also display decreased spine density and synapse formation (Sala, 2016). To test this with human neurons, NPCs were differentiated for eight weeks before imaging, so as to reach a developmental stage resembling that of mid-fetal neurons *in vivo*. After six weeks of differentiation, the neurons were transduced with a lentiviral vector to introduce a Synapsin-GFP construct for visualization during imaging (**Fig 5A-C**). The neurons were imaged for a total of 60 minutes at 30 second intervals, and their dendritic spines were quantified and measured. There was no significant difference measured in the number of spines that formed, became extinct, or stayed stable between CDKL5 and control neurons (**Fig 5D-F**). However, CDKL5 neurons exhibited a significantly higher density of dendritic spines as compared to controls (**Fig 5G**). As CDKL5 has also been implicated in a decrease in synapse formation (La Montanara, 2015), the lengths of individual spines were also measured to extrapolate information about the rates at which their lengths were changing (**Fig 5H**). CDKL5 neuronal spines appeared to have greater motility compared to controls, displaying a significantly greater movement speed (**Fig 5I**). In conclusion, the data from this experiment using human iPSC-derived neurons appear to contradict the previous findings from murine studies regarding the parameters of spine density and motility.

DISCUSSION

hiPSCs present an unparalleled opportunity to study the effects of neurodevelopmental diseases on human neurons in a controlled setting. Having the ability to culture cells that retain the same genetic information of patients allows for valid comparison and testing, while avoiding the possibility of extraneous mutations during genome editing. Furthermore, it circumvents the issue of gene function not being conserved across species that animal models might face.

Although the function of the CDKL5 protein remains largely unknown, there have been strong connections made between it and the AKT pathway (Fuchs, 2014), as well as the mTOR pathway (Wang, 2012), of which AKT is an upstream element. As the AKT pathway plays a large role in the control of cellular proliferation and apoptosis (Yu, 2016), CDKL5 mutant neural progenitor cells were analyzed for cell cycling, proliferation, and apoptosis. Furthermore, the AKT/mTOR pathway has been shown to be involved in dendritic growth and synapse formation (La Montanara, 2015), both of which are important for neuronal communication. Therefore, neurons differentiated from patient-derived iPSCs were examined using these parameters.

When examining the characteristics of cells before the mid-fetal stage of maturation, hiPSCs prove to be an extremely robust model. Therefore, it was decided to perform various assays on neural progenitor cells to explore the connections between CDKL5 and the AKT/mTOR pathways. Previous studies have shown that the AKT pathway heavily involved in cell proliferation and survival in cancer cells (Yu, 2016; Osaki, 2015). To examine the relationship between the CDKL5 protein and this pathway, Fuchs and colleagues employed a CDKL5 knockout murine model, which showed an increase in apoptosis of neural cell precursors, as well as a higher rate of precursor cell

proliferation. The data from this study agree with the increased apoptotic rate in CDKL5 mutant NPCs but found the opposite in proliferative rate; CDKL5 mutant NPCs were less proliferative than controls. It is possible that this discrepancy might be due to species-specific differences in CDKL5 protein function, as human cancer cells display an increase of cell proliferation and a decrease in apoptosis upon overactivation of this pathway (Yu, 2016). Therefore, the CDKL5 loss of function mutation may have led to a decrease in activation of the AKT/mTOR pathways, resulting in the decrease of NPC proliferation and an increase in apoptosis. The lack of a significant difference in the apoptotic rates of D135_F154del NPCs proves interesting as it suggests the aberrantly spliced CDKL5 protein might retain some function, preventing the significant increase in NPC apoptosis.

Previous studies have shown that neurons afflicted with neurodevelopmental disease tend to exhibit aberrant patterns of synapse formation and spine function (La Montanara, 2015; Marchetto, 2010). Furthermore, neurodevelopmental disease also commonly results in abnormal levels of neurodegeneration (Laplante & Sabatini, 2012). Two and eight-week Neurons were analyzed to determine possible effects of the CDKL5 protein on dendritic growth and spine dynamics respectively. CDKL5 mutant neurons exhibited slower dendritic growth during early neurodevelopment but no difference in total dendritic length. They also had a greater density of dendritic spines that had greater motility than controls, though there was not a significant difference in the other parameters for spine dynamics that were recorded: formation, extinction, and stable spines. The increased motility is likely due to the decreased ability of CDKL5 neurons to

form synapses (La Montanara, 2015), resulting in increased attempts of the isolated neuron to make connections.

Surprisingly, these results contrast those of previous murine studies, which found that neurons from CDKL5-knockout mice had decreased total dendritic length, as well as reduced spine density and motility (La Montanara, 2015; Marchetto, 2010; Chen, 2010). Despite the benefits of utilizing iPSC derived neurons for study, the limitations of this technology must be recognized. The protocol used to generate neurons in this study produces primarily cortical neurons, all of which only reach the maturation analogous to the mid-fetal stage. As such, though the results from the neurite outgrowth experiments reveal growth patterns during early neurodevelopment, a different model must be utilized to study how these growth patterns change as the neurons continue to mature. La Montanara and colleagues harvested cortical slices from the brains of adult CDKL5-knockout mice, allowing them to study neurons that had fully matured *in vivo*. Another possible explanation for this difference could be that the function of the CDKL5 protein may not be fully conserved across species. Support for this theory is especially supported by the inability of murine models to recapitulate the defining feature of CDKL5 syndrome in humans; early-onset intractable seizures (Wang, 2012). Furthermore, Hector and colleagues discovered that there is only a conservation of 29-42% CDKL5 sequence identity between mice and human due to species-specific alternative splicing (Hector, 2016).

The advent of iPSC technology has allowed researchers to overcome the variability and challenges associated with genome editing, as well as the difficulty of obtaining inaccessible samples such as cortical neurons. However, there are inherent

limitations to this technology, especially with regards to cellular maturation. This study has worked within these limitations to elucidate trends regarding the early neurodevelopment of CDKL5 mutant iPSCs. Although the results may more accurately capture these trends due to the human nature of the cellular model, the advantages of utilizing an animal model cannot be ignored. Performing disease modeling using both an iPSC and animal model side-by-side is a potential method of increasing the robustness of the acquired results, although it would not be able to overcome any interspecies genetic differences. A promising new technology that is emerging to combat this issue is the use of chimeric animals. By allowing hiPSC-derived cells to mature *in-vivo* before harvesting, one can circumvent the limitations on maturing cells *in-vitro* while preserving the human genetic profile. However, there are ethical concerns surrounding implanting human cells, especially neural cells, into an animal. Furthermore, it is possible that the *in-vivo* environment may alter the phenotype of the human cells in some way. Despite these challenges, the use of chimeric animals to model disease has great potential in furthering the study of genetic diseases that may not translate across species, as might be the case with CDKL5.

In summary, this study has used hiPSC derived neural progenitors and neurons to study the effects of CDKL5 deficiency in several downstream targets of the AKT/mTOR pathway: cellular proliferation, apoptosis, dendritic outgrowth, and spine motility. The data served to corroborate findings from human studies of these pathways but conflicted with the results from studies of CDKL5 disorder using murine models. Hopefully, this discrepancy in the results will prompt other researchers to explore the possibility of

differences in CDKL5 protein function across species, as well as support the validity of using hiPSC models to study early neurodevelopment.

FIGURES

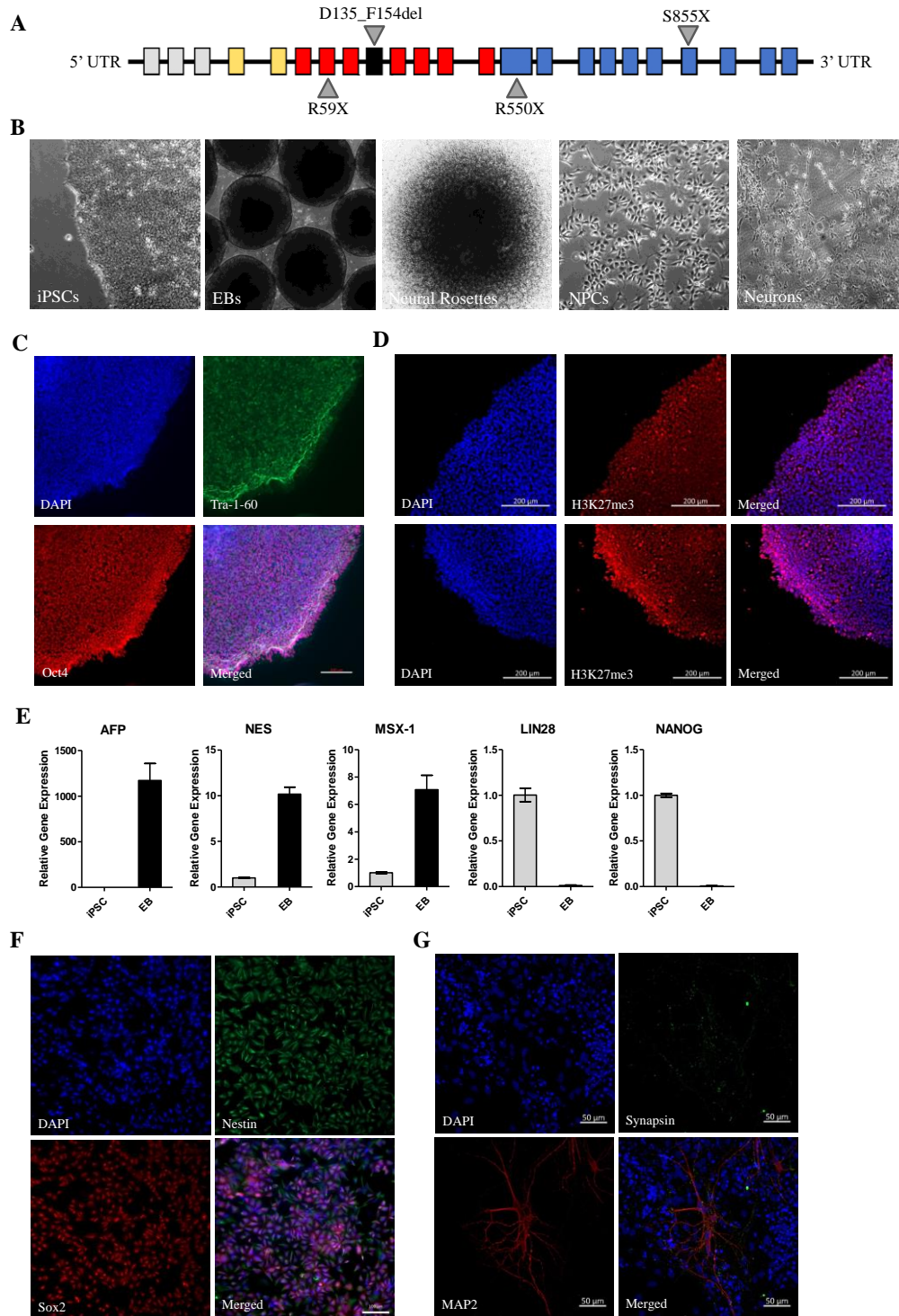


Figure 1. Characterization of CDKL5 disorder patient-derived iPSCs and their potential for differentiation. **A.** Schematic representing the structure of the CDKL5 gene, as well as the associated mutations of the patient cells used in this study. Exons 1, 1a, and 1b (grey) are noncoding. Exons 2 and 3 (yellow) code for the ATP binding site. Exons 4-6 and 8-11 (red) code for the serine/threonine kinase domain, while exon 7

Figure 1. Continued

(black) codes for the active site of the CDKL5 protein. Exons 12-21 (blue) comprise the C-terminal domain. **B.** Representative images for each step of the neural induction protocol. **C.** Representative immunofluorescence images of various iPSC markers. **D.** Representative immunofluorescence images comparing state of H3K27me3 methylation (X inactivation) for an isogenic cell line pair. **E.** Relative gene expression of several developmental proteins in iPSCs and EBs. AFP (endoderm), NES (ectoderm), and MSX1 (mesoderm) serve as cell lineage markers, while LIN28 and NANOG serve as pluripotency markers. **F.** Representative immunofluorescence images of various NPC markers. **G.** Representative immunofluorescence images of various neuronal markers.

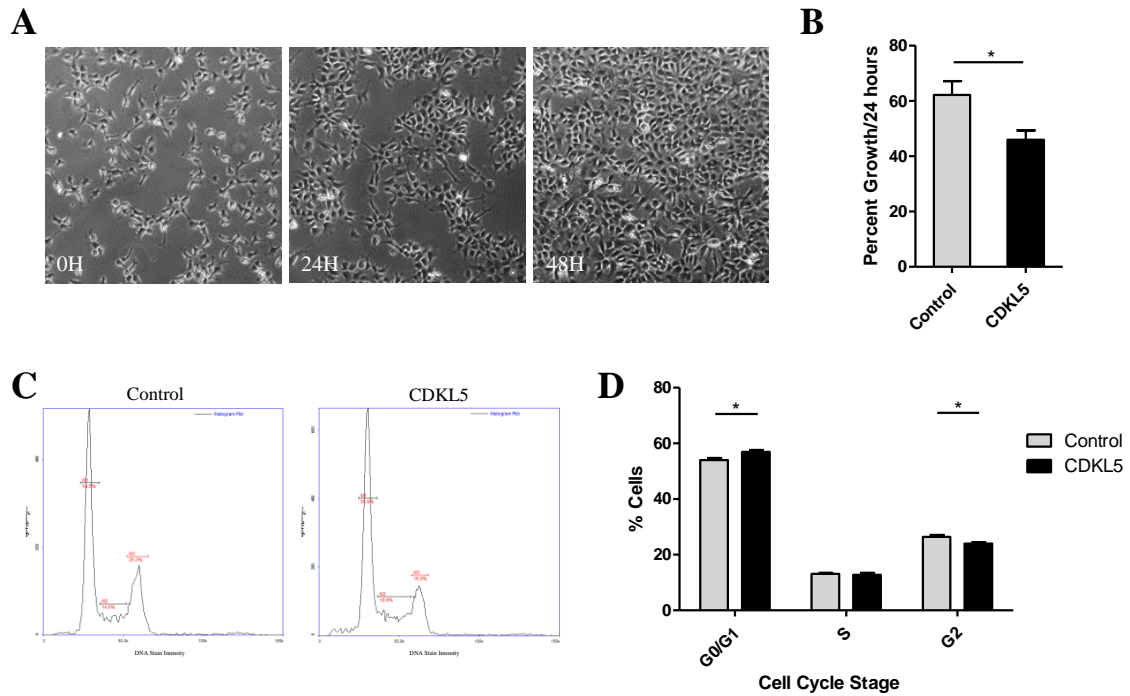


Figure 2. NPCs derived from CDKL5 disorder patient iPSCs display decreased levels of proliferation. **A.** Representative bright field images of 2D plated NPCs live-imaged over a 48-hour period (0H, 24H, and 48H images shown). Images were taken at 20x magnification. **B.** The growth rate of NPCs over 24 hour periods was compared. **C.** Representative images of NPC cell cycle profiles of Control (left) and CDKL5 (right) NPCs. Markers in the diagrams are used to denote different stages of the cell cycle. **D.** Percentage of Control (grey) and CDKL5 (black) cells within each stage of the cell cycle. All data are presented as the mean \pm SEM; n = 3. n, number of cells lines used with their associated controls. * $p < 0.05$, two-tailed unpaired t-test.

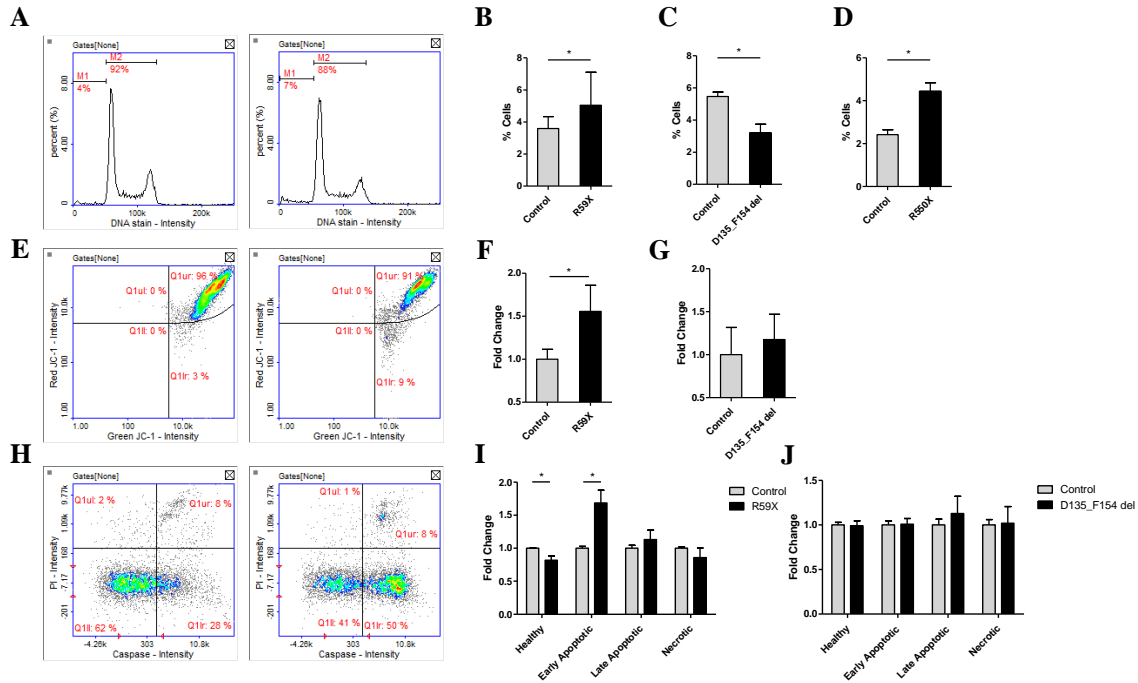


Figure 3. CDKL5 Disorder leads to increased levels of apoptosis in NPCs. **A.** Images from the DAPI staining assay used to determine levels of DNA fragmentation in cells. Both the control (left) and CDKL5 (right) cell lines are represented. Markers denote the percentage of cells with fragmented and unfragmented DNA. **B.** Percent of cells from R59X cell lines that have fragmented DNA. $n=2$, where n denotes the number of cell line pairs. **C.** Percent of cells from the D135_F154del cell line that have fragmented DNA. $n=1$, where n denotes the number of cell line pairs. **D.** Percent of cells from the R550X isogenic cell line that have fragmented DNA. $n=1$, where n denotes the number of cell line pairs. **E.** Images from the JC-1 assay for mitochondrial depolarization. Quadrants represent different cell populations. **F.** Relative amount of cells with depolarized mitochondria between R59X cells and related controls. $n=2$, where n denotes the number of cell line pairs. **G.** Relative amount of cells with depolarized mitochondria between D135_F154del cells and related controls. $n=1$, where n denotes the number of cell line pairs. **H.** Images from the caspase staining assay to determine levels of apoptotic cells. Each quadrant represents a different cell population. **I.** Relative amount of apoptotic cell populations between R59X cells and related controls. $n=2$, where n denotes the number of cell line pairs. **J.** Relative amount of apoptotic cell populations between D135_F154del cells and related controls. $n=1$, where n denotes the number of cell line pairs. For all graphs, the columns represent the mean, and error bars denote SEM. * $p<0.05$, two-tailed unpaired t-test.

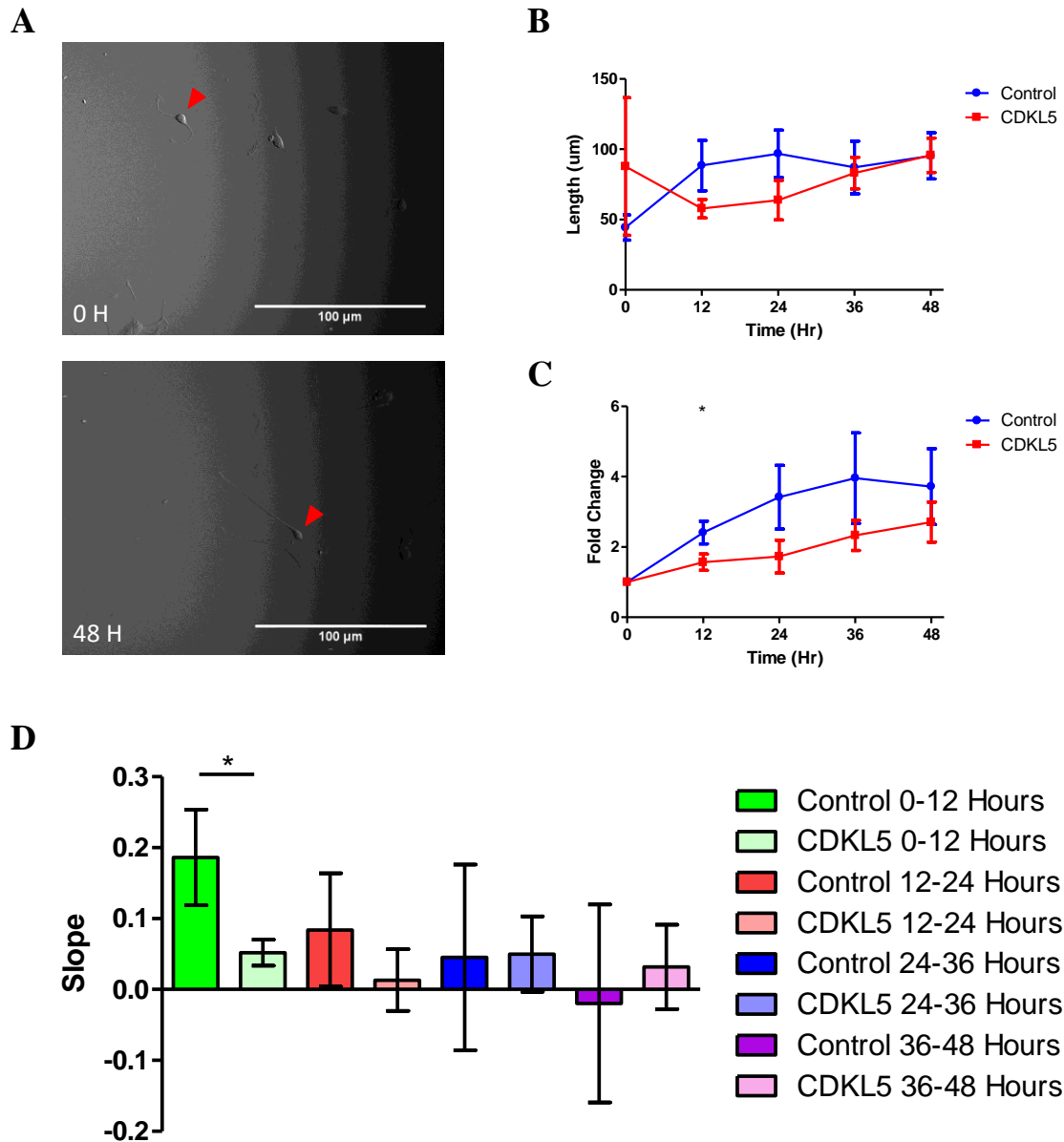


Figure 4. CDKL5 disorder iPSC-derived neurons appear to grow more slowly than controls during early development. **A.** Representative bright field image of a neuron tracked over a 48-hour period (red arrow). **B.** Total length of all neurites from CDKL5 and control neurons over 48 hours. **C.** The relative amount of change in total length of all neurites between CDKL5 and control neurons over a 48-hour period as compared to the total length at t=0H. **D.** Comparison of the slopes (representing growth rate) between several time points: 0-12 hours, 12-24 hours, 24-36 hours, and 36-48 hours. All data are presented as the mean \pm SEM; n = 14. n, number of neurons analyzed per 12-hour time interval, along with their associated controls. * $p < 0.05$, two-tailed unpaired t-test.

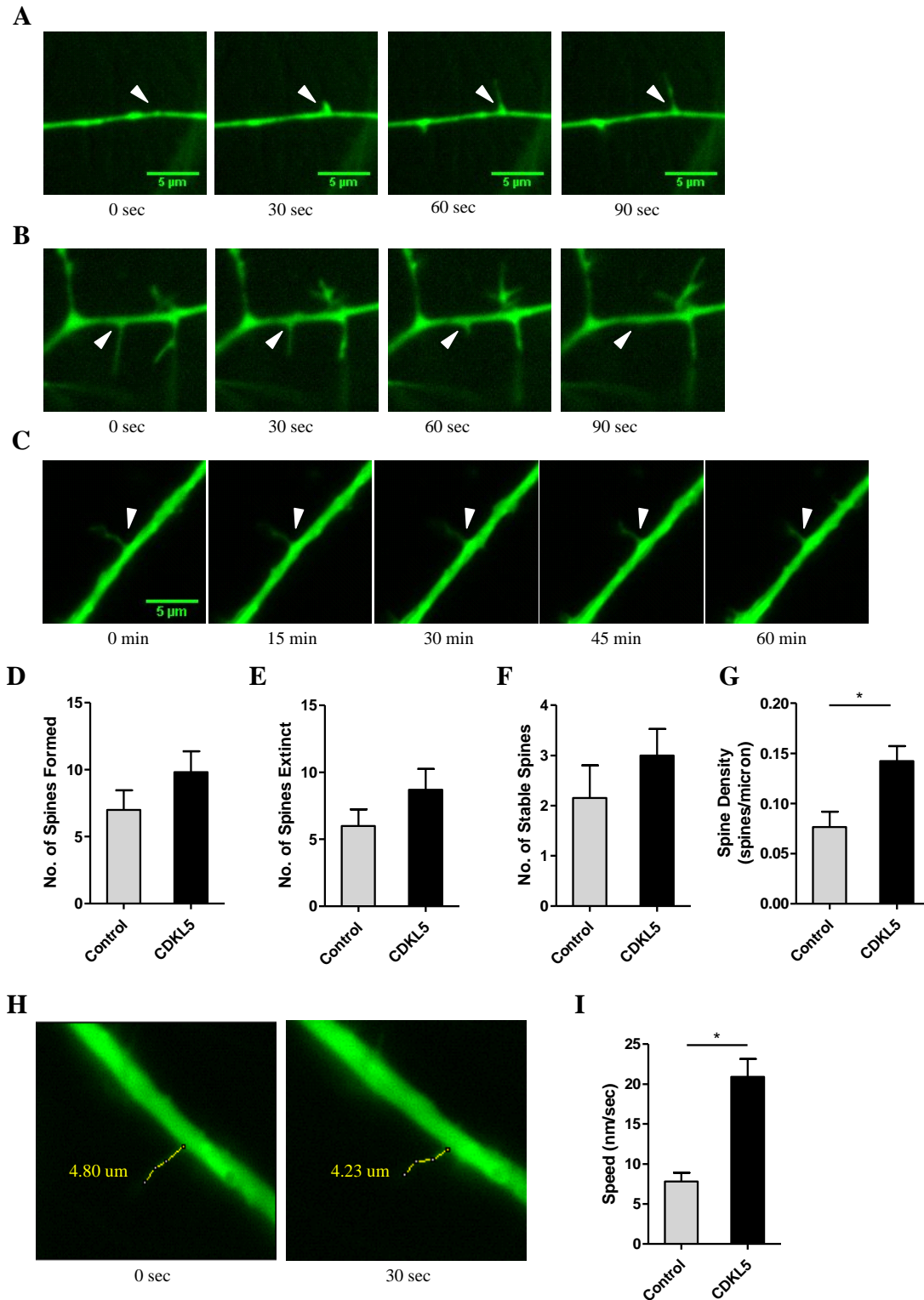


Figure 5. CDKL5 disorder iPSC-derived neurons display a greater density of spines with increased motility. A-C. Representative immunofluorescent images of CDKL5 neurons after 8 weeks of differentiation. The white arrows denote spines that are forming (A), going extinct (B), and remaining stable (C). Formation and extinction are shown

Figure 5. Continued

over a 90 second time course whereas stability is displayed over a 60-minute time course. **D.** Total number of spines that were formed during a 60 minute live-imaging. **E.** Total number of spines that became extinct during a 60 minute live-imaging. **F.** Total number of spines that were stable over 60 minutes of live-imaging. **G.** The spine density measured as the number of spines present per micron of neurite at 15-minute intervals across 60 minutes of live-imaging. **H.** Representative immunofluorescent image showing the measurement of the length of a spine using NeuronJ. The tracing (yellow line) is overlaying a spine at t=0 (left) and t=30sec (right), with the associated lengths denoted adjacent. **I.** The relative speeds of spine movement presented in nanometers/second. All data are presented as the mean \pm SEM; n = 14. n, number of neurons analyzed per condition, along with their associated controls. *p<0.05, two-tailed unpaired t-test.

TABLES

Table 1. CDKL5 Patient Cohort and Controls.

Cell Line	Condition	Mutation	Gender	Age	Relationship	Exon
3	CDKL5	R59X	Female	3	Daughter	5
4	Control	None	Female	41	Mother of Patient 3	None
10	CDKL5	R59X	Male	15	Son	5
11	Control	None	Male	35	Father of Patient 10	None
91	CDKL5	D153_F154del	Male	4	Son	7
101	Control	None	Male	38	Father of Patient 91	None
122C1	CDKL5	R550X	Female	3	Patient 122	12
122C2	Control	None	Female	3	Isogenic control of Patient 122	None

REFERENCES

- Alessio N, Capasso S, Ferone A, Bernardo GD, Cipollaro M, Casale F, Peluso G, Giordano A, Galderisi U. Misidentified Human Gene Functions with Mouse Models: The Case of the Retinoblastoma Gene Family in Senescence. *Neoplasia*. 2017;19(10):781-790. doi:10.1016/j.neo.2017.06.005.
- Amendola E, Zhan Y, Mattucci C, Castroflorio E, Calcagno E, Fuchs C, Lonetti G, Silingardi D, Vyssotski AL, Farley D, Ciani E, Pizzorusso T, Giustetto M, Gross CT. Mapping Pathological Phenotypes in a Mouse Model of CDKL5 Disorder. *PLoS ONE*. 2014;9(5). doi:10.1371/journal.pone.0091613.
- Amir RE, Veyver IBVD, Wan M, Tran CQ, Francke U, Zoghbi HY. Rett syndrome is caused by mutations in X-linked MECP2, encoding methyl-CpG-binding protein 2. *Nature Genetics*. 1999;23(2):185-188. doi:10.1038/13810.
- Ananiev G, Williams EC, Li H, Chang Q. Isogenic Pairs of Wild Type and Mutant Induced Pluripotent Stem Cell (iPSC) Lines from Rett Syndrome Patients as In Vitro Disease Model. *PLoS ONE*. 2011;6(9). doi:10.1371/journal.pone.0025255.
- Bahi-Buisson N, Bienvenu T. CDKL5-Related Disorders: From Clinical Description to Molecular Genetics. *Molecular Syndromology*. 2011. doi:10.1159/000331333.
- Bahi-Buisson N, Kaminska A, Boddaert N, Rio M, Afenjar A, Gérard M, Giuliano F, Motte J, Héron D, Morel MAN, Plouin P, Richelme C, Portes VD, Dulac O, Philippe C, Chiron C, Nabbout R, Bienvenu T. The three stages of epilepsy in patients with CDKL5 mutations. *Epilepsia*. 2008;49(6):1027-1037. doi:10.1111/j.1528-1167.2007.01520.x.
- Bente D, Gren J, Strong JE, Feldmann H. Disease modeling for Ebola and Marburg viruses. *Disease Models and Mechanisms*. 2009;2(1-2):12-17. doi:10.1242/dmm.000471.
- Bestor TH. The DNA methyltransferases of mammals. *Human Molecular Genetics*. 2000;9(16):2395-2402. doi:10.1093/hmg/9.16.2395.
- Bolker J. There's more to life than rats and flies. *Nature*. 2012;491(7422):31-33. doi:10.1038/491031a.
- Cammalleri M, Lutjens R, Berton F, King AR, Simpson C, Francesconi W, Sanna PP. Time-restricted role for dendritic activation of the mTOR-p70S6K pathway in the induction of late-phase long-term potentiation in the CA1. *Proceedings of the*

National Academy of Sciences. 2003;100(24):14368-14373.
doi:10.1073/pnas.2336098100.

Carouge D, Host L, Aunis D, Zwiller J, Anglard P. CDKL5 is a brain MeCP2 target gene regulated by DNA methylation. *Neurobiology of Disease*. 2010;38(3):414-424.
doi:10.1016/j.nbd.2010.02.014.

Chen Q, Zhu Y-C, Yu J, Miao S, Zheng J, Xu L, Zhou Y, Li D, Zhang C, Tao J, Xiong Z-Q. CDKL5, a Protein Associated with Rett Syndrome, Regulates Neuronal Morphogenesis via Rac1 Signaling. *Journal of Neuroscience*. 2010;30(38):12777-12786. doi:10.1523/jneurosci.1102-10.2010.

Ebert AD, Liang P, Wu JC. Induced Pluripotent Stem Cells as a Disease Modeling and Drug Screening Platform. *Journal of Cardiovascular Pharmacology*. 2012;60(4):408-416. doi:10.1097/fjc.0b013e318247f642.

Fehr S, Wilson M, Downs J, Williams S, Murgia A, Sartori S, Vecchi M, Ho G, Polli R, Psoni S, Bao X, Klerk ND, Leonard H, Christodoulou J. The CDKL5 disorder is an independent clinical entity associated with early-onset encephalopathy. *European Journal of Human Genetics*. 2012;21(3):266-273. doi:10.1038/ejhg.2012.156.

Ferrer I, Martinez A, Boluda S, Parchi P, Barrachina M. Brain banks: benefits, limitations and cautions concerning the use of post-mortem brain tissue for molecular studies. *Cell and Tissue Banking*. 2008;9(3):181-194. doi:10.1007/s10561-008-9077-0.

Fuchs C, Trazzi S, Torricella R, Viggiano R, Franceschi MD, Amendola E, Gross C, Calzà L, Bartesaghi R, Ciani E. Loss of CDKL5 impairs survival and dendritic growth of newborn neurons by altering AKT/GSK-3 β signaling. *Neurobiology of Disease*. 2014;70:53-68. doi:10.1016/j.nbd.2014.06.006.

Grider M, Park D, Spencer D, Shine H. Lipid raft-targeted Akt promotes axonal branching and growth cone expansion via mTOR and Rac1, respectively. *Journal of Neuroscience Research*. 2009;87(14):3033-3042. doi:10.1002/jnr.22140.

Hagberg B. Clinical manifestations and stages of rett syndrome. *Mental Retardation and Developmental Disabilities Research Reviews*. 2002;8(2):61-65.
doi:10.1002/mrdd.10020.

Hector RD, Dando O, Landsberger N, Kilstrup-Nielsen C, Kind PC, Bailey MES, Cobb SR. Characterisation of CDKL5 Transcript Isoforms in Human and Mouse. *Plos One*. 2016;11(6). doi:10.1371/journal.pone.0157758.

- Herrath MG, Nepom GT. Lost in translation: Figure 1. *The Journal of Experimental Medicine*. 2005;202(9):1159-1162. doi:10.1084/jem.20051224.
- Kameshita I, Sekiguchi M, Hamasaki D, Sugiyama Y, Hatano N, Suetake I, Tajima S, Sueyoshi N. Cyclin-dependent kinase-like 5 binds and phosphorylates DNA methyltransferase 1. *Biochemical and Biophysical Research Communications*. 2008;377(4):1162-1167. doi:10.1016/j.bbrc.2008.10.113.
- Kobayashi T, Taguchi K, Yasuhiro T, Matsumoto T, Kamata K. Impairment of PI3-K/Akt Pathway Underlies Attenuated Endothelial Function in Aorta of Type 2 Diabetic Mouse Model. *Hypertension*. 2004;44(6):956-962. doi:10.1161/01.hyp.0000147559.10261.a7.
- Laplanche M, Sabatini DM. mTOR Signaling in Growth Control and Disease. *Cell*. 2012;149(2):274-293. doi:10.1016/j.cell.2012.03.017.
- Marchetto MC, Carroneu C, Acab A, Yu D, Yeo GW, Mu Y, Chen G, Gage FH, Muotri AR. A Model for Neural Development and Treatment of Rett Syndrome Using Human Induced Pluripotent Stem Cells. *Cell*. 2010;143(4):527-539. doi:10.1016/j.cell.2010.10.016.
- Meijering E, Jacob M, Sarría J-C, Steiner P, Hirling H, Unser M. Design and validation of a tool for neurite tracing and analysis in fluorescence microscopy images. *Cytometry*. 2004;58A(2):167-176. doi:10.1002/cyto.a.20022.
- Montanara PL, Rusconi L, Locarno A, Forti L, Barbiero I, Tramarin M, Chandola C, Kilstrup-Nielsen C, Landsberger N. Synaptic Synthesis, Dephosphorylation, and Degradation. *Journal of Biological Chemistry*. 2015;290(7):4512-4527. doi:10.1074/jbc.m114.589762.
- Nageshappa S, Carroneu C, Trujillo CA, Mesci P, Espuny-Camacho I, Pasciuto E, Vanderhaeghen P, Verfaillie CM, Raitano S, Kumar A, Carvalho CMB, Bagni C, Ramocki MB, Araujo BHS, Torres LB, Lupski JR, Esch HV, Muotri AR. Altered neuronal network and rescue in a human MECP2 duplication model. *Molecular Psychiatry*. 2015;21(2):178-188. doi:10.1038/mp.2015.128.
- Osaki M, Oshimura M, Ito H. PI3K-Akt pathway: Its functions and alterations in human cancer. *Apoptosis*. 2004;9(6):667-676. doi:10.1023/b:appt.0000045801.15585.dd.
- Paşca SP, Portmann T, Voineagu I, Yazawa M, Shcheglovitov A, Paşca AM, Cord B, Palmer TD, Chikahisa S, Nishino S, Bernstein JA, Hallmayer J, Geschwind DH, Dolmetsch RE. Using iPSC-derived neurons to uncover cellular phenotypes

associated with Timothy syndrome. *Nature Medicine*. 2011;17(12):1657-1662.
doi:10.1038/nm.2576.

Ricciardi S, Ungaro F, Hambrock M, Rademacher N, Stefanelli G, Brambilla D, Sessa A, Magagnotti C, Bachi A, Giarda E, Verpelli C, Kilstrup-Nielsen C, Sala C, Kalscheuer VM, Broccoli V. CDKL5 ensures excitatory synapse stability by reinforcing NGL-1–PSD95 interaction in the postsynaptic compartment and is impaired in patient iPSC-derived neurons. *Nature Cell Biology*. 2012;14(9):911-923.
doi:10.1038/ncb2566.

Sala GD, Putignano E, Chelini G, Melani R, Calcagno E, Ratto GM, Amendola E, Gross CT, Giustetto M, Pizzorusso T. Dendritic Spine Instability in a Mouse Model of CDKL5 Disorder Is Rescued by Insulin-like Growth Factor 1. *Biological Psychiatry*. 2016;80(4):302-311. doi:10.1016/j.biopsych.2015.08.028.

Schindelin J, Arganda-Carreras I, Frise E, Kaynig V, Longair M, Pietzsch T, Preibisch S, Rueden C, Saalfeld S, Schmid B, Tinevez J-Y, White DJ, Hartenstein V, Eliceiri K, Tomancak P, Cardona A. Fiji: an open-source platform for biological-image analysis. *Nature Methods*. 2012;9(7):676-682. doi:10.1038/nmeth.2019.

Soldner F, Jaenisch R. iPSC Disease Modeling. *Science*. 2012;338(6111):1155-1156.
doi:10.1126/science.1227682.

Stein JL, De La Torre-Ubieta L, Tian Y, Parikhshak NN, Hernández IA, Marchetto MC, Baker DK, Lu D, Hinman CR, Lowe JK, Wexler EM, Muotri AR, Gage FH, Kosik KS, Geschwind DH. A Quantitative Framework to Evaluate Modeling of Cortical Development by Neural Stem Cells. *Neuron*. 2014;83(1):69-86.
doi:10.1016/j.neuron.2014.05.035.

Takahashi K, Tanabe K, Ohnuki M, Narita M, Ichisaka T, Tomoda K, Yamanaka S. Induction of Pluripotent Stem Cells From Adult Human Fibroblasts by Defined Factors. *Obstetrical & Gynecological Survey*. 2008;63(3):153.
doi:10.1097/01.ogx.0000305204.97355.0d.

Thomson JA. Embryonic Stem Cell Lines Derived from Human Blastocysts. *Science*. 1998;282(5391):1145-1147. doi:10.1126/science.282.5391.1145.

Tropea D, Giacometti E, Wilson NR, Beard C, Mccurry C, Fu DD, Flannery R, Jaenisch R, Sur M. Partial reversal of Rett Syndrome-like symptoms in MeCP2 mutant mice. *Proceedings of the National Academy of Sciences*. 2009;106(6):2029-2034.
doi:10.1073/pnas.0812394106.

Wang I-TJ, Allen M, Goffin D, Zhu X, Fairless AH, Brodtkin ES, Siegel SJ, Marsh ED, Blendy JA, Zhou Z. Loss of CDKL5 disrupts kinome profile and event-related potentials leading to autistic-like phenotypes in mice. *Proceedings of the National Academy of Sciences*. 2012;109(52):21516-21521. doi:10.1073/pnas.1216988110.

Watase K, Zoghbi HY. Modelling brain diseases in mice: the challenges of design and analysis. *Nature Reviews Genetics*. 2003;4(4):296-307. doi:10.1038/nrg1045.

Yu JSL, Cui W. Proliferation, survival and metabolism: the role of PI3K/AKT/mTOR signalling in pluripotency and cell fate determination. *Development*. 2016;143(17):3050-3060. doi:10.1242/dev.137075.